

High-performance spin-filtering and spin-rectifying effects in Blatter radical-based molecular spintronic device

Chun-Xu Tong(童春旭), Peng Zhao(赵朋), and Gang Chen(陈刚)

Citation: Chin. Phys. B, 2023, 32 (**6**): 067202. DOI: 10.1088/1674-1056/acc16d
Journal homepage: http://cpb.iphy.ac.cn; http://iopscience.iop.org/cpb

What follows is a list of articles you may be interested in

Interface-induced topological phase and doping-modulated bandgap of two-dimensioanl graphene-like networks

Ningjing Yang(杨柠境), Hai Yang(杨海), and Guojun Jin(金国钧)
Chin. Phys. B, 2023, 32 (**1**): 017201. DOI: 10.1088/1674-1056/ac904d

Current spin polarization of a platform molecule with compression effect

Zhi Yang(羊志), Feng Sun(孙峰), Deng-Hui Chen(陈登辉), Zi-Qun Wang(王子群), Chuan-Kui Wang(王传奎), Zong-Liang Li(李宗良), and Shuai Qiu(邱帅)
Chin. Phys. B, 2022, 31 (**7**): 077202. DOI: 10.1088/1674-1056/ac4f53

Theoretical design of thermal spin molecular logic gates by using a combinational molecular junction

Yi Guo(郭逸), Peng Zhao(赵朋), and Gang Chen(陈刚)
Chin. Phys. B, 2022, 31 (**4**): 047202. DOI: 10.1088/1674-1056/ac3a5f

Recent spinterfacial studies targeted to spin manipulation in molecular spintronic devices

Xian-Rong Gu(谷现荣), Li-Dan Guo(郭立丹), Xiang-Nan Sun(孙向南)
Chin. Phys. B, 2018, 27 (**10**): 107202. DOI: 10.1088/1674-1056/27/10/107202

Spin-filter effect and spin-polarized optoelectronic properties in annulene-based molecular spintronic devices

Zhiyuan Ma(马志远), Ying Li(李莹), Xian-Jiang Song(宋贤江), Zhi Yang(杨致), Li-Chun Xu(徐利春), Ruiping Liu(刘瑞萍), Xuguang Liu(刘旭光), Dianyin Hu(胡殿印)
Chin. Phys. B, 2017, 26 (**6**): 067201. DOI: 10.1088/1674-1056/26/6/067201

High-performance spin-filtering and spin-rectifying effects in Blatter radical-based molecular spintronic device

Chun-Xu Tong(童春旭)[1], Peng Zhao(赵朋)[1,†], and Gang Chen(陈刚)[2]

[1] *School of Physics and Technology, University of Jinan, Jinan* 250022, *China*
[2] *School of Physics and Electronics, Shandong Normal University, Jinan* 250358, *China*

(Received 5 December 2022; revised manuscript received 3 March 2023; accepted manuscript online 5 March 2023)

We design a Blatter radical-based molecular spintronic device, and investigate its spin-polarized transport properties using density functional theory and non-equilibrium Green's function technique. High-performance spin-rectifying and spin-filtering effects are realized. The physical mechanism is explained by the spin-resolved bias voltage-dependent transmission spectra, the energy levels of the corresponding molecular projected self-consistent Hamiltonian orbitals, and their spatial distributions. The results demonstrate that the Blatter radical has great potential in the development of high-performance multifunctional molecular spintronic devices.

Keywords: spin-filtering, spin-rectifying, molecular spintronic device, Blatter radical

PACS: 72.25.–b, 85.65.+h, 85.75.–d **DOI:** 10.1088/1674-1056/acc16d

1. Introduction

Due to the technical and physical limitations of traditional silicon-based electronic technology, molecular devices have become one of the best inheritors of silicon-based devices. Up to now, researchers have proposed and constructed many nanoelectronic devices based on single molecules with specific functions, such as rectifying,[1,2] sensing,[3,4] switching,[5,6] negative differential resistance (NDR),[7,8] and so on. Among them, molecular rectifier has attracted much attention because it is the core component of molecular logic circuit. In fact, the concept of molecular rectifier can be dated back to 1974 with Aviram and Ratner's ground-breaking theoretical work of realizing molecular rectifying effect in an asymmetric molecule.[9] Since then, much effort has been devoted to the study of molecular rectifiers. In general, in order to achieve the molecular rectifying effect, the molecular orbitals (MOs) near Fermi level ($E_{\rm F}$) should have different coupling strengths with the left and right electrodes, and respond differently to the forward and backward bias voltages. At present, one of the important tasks in the research of molecular rectifier is to search for appropriate molecular materials which can realize large rectifying ratio.

At the same time, it is well known that compared with traditional electronic devices, the use of electron spin to carry information can greatly improve data processing speed, enhance integration density, reduce energy consumption, and thus significantly improve devices' performance. Therefore, molecular spintronic devices (MSDs) have become the research hotspot of next-generation electronic devices in recent years.[10–13] The key to the development of MSDs is to search for suitable magnetic molecular materials which can generate highly spin-polarized current with long spin coherence length (SCL). Organic radicals of light elements, with unpaired valence electrons or an open electron shell, are particularly suited to this requirement. On the one hand, the spin-polarized MOs of organic radicals around the $E_{\rm F}$ are markedly split, resulting in the energy level of one spin orientation closer to the $E_{\rm F}$ and higher transmission, which may result in a highly spin-polarized current. On the other hand, the weak spin–orbit coupling and hyperfine interactions in organic radicals can give rise to long SCL. Based on these facts, Herrmann *et al*. first discussed how simple π-type organic radicals may function as spin filters and how they may be adjusted by adding appropriate substituents to filter either spin-up or spin-down electrons.[14] Smeu *et al*. further studied the spin-filtering performance of various σ- and π-type organic radicals.[15] Shil *et al.* showed that a high-spin organic diradical can also act as a spin filter.[16] Bajaj *et al*. reported anomalous quantum interference effect in spin filters based on organic radicals.[17] Recently, Smeu *et al*. demonstrated that two kinds of phenalenyl-based radicals can preserve a high spin-filtering performance up to 0.4 V.[18] Very recently, we found that a highly spin-polarized current can be achieved in 1,3,5-triphenylverdazyl (TPV) radical by linkage mode modulation.[19]

The 1,2,4-benzotriazinyl radical, also known as Blatter radical, was developed by Blatter in 1968.[20] In contrast to the instability of most free radicals, Blatter radical is so stable that it can be stored in ambient conditions for months.[21–23] Over the last years, Blatter radical and its derivatives have attracted more and more attention as molecular magnet, polymerization mediator or potential quantum bit in quantum computer.[24–28] In the present work, we design a Blatter radical-based MSD

†Corresponding author. E-mail: ss_zhaop@ujn.edu.cn

© 2023 Chinese Physical Society and IOP Publishing Ltd

and investigate its spin-polarized transport properties using a first-principles method based on the density functional theory (DFT) combined with the non-equilibrium Green's function (NEGF) technique. Our results show that the designed MSD can exhibit high-performance spin-filtering and spin-rectifying effects. In the following parts of this article, theoretical model and computational details are given in Section 2. Numerical results and discussion are presented in Section 3. Finally, a conclusion is given in Section 4.

2. Theoretical model and computational details

Figure 1 depicts the model structure of the designed MSD, in which a Blatter radical is coupled covalently to two gold electrodes in the (111) direction via sulfur atom on the hollow site.[29–31] Our model is divided into three regions: the left electrode (LE), the central scattering region (CSR), and the right electrode (RE). Each layer of LE and RE is modeled by a transverse (5×5) supercell with periodic boundary conditions to ensure that it can simulate bulk metal structures. The CSR contains the Blatter radical, two anchoring sulfur atoms and part of gold electrodes. The distance between LE and RE is obtained by the total energy optimization of a series of different fixed electrode–electrode spacing using the Limited memory Broyden–Fletcher–Goldfarb–Shanno (LBFGS) method. During the optimization process, the geometries of the Blatter radical and two anchoring sulfur atoms are relaxed to a force tolerance of 0.04 eV/Å, while keeping the gold electrodes fixed. Then the spin-polarized current through the MSD is calculated in the framework of the Landauer–Büttiker approximation according to the following equation:[32]

$$I_\sigma = \frac{e}{h}\int T_\sigma(E,V)[f(E-\mu_{\rm L})-f(E-\mu_{\rm R})]\,{\rm d}E, \qquad (1)$$

here spin index $\sigma = {\rm up/dn}$ represents the spin-up/spin-down. e and h are the electron charge and Planck constant, respectively. $f(E-\mu_{\rm L/R})$ is the Fermi–Dirac distribution function of LE/RE. $\mu_{\rm L} = E_{\rm F} - eV/2$ and $\mu_{\rm R} = E_{\rm F} + eV/2$ are the chemical potential of LE and RE, where $E_{\rm F}$ is the Fermi level, and it has been set to the energy origin in the simulations for clarity. $T_\sigma(E,V)$ is the bias voltage-dependent spin-resolved transmission coefficient related to energy and bias voltage. Obviously, I_σ depends on the integral of $T_\sigma(E,V)$ in the energy range $[-eV/2, eV/2]$. This energy range is called the bias voltage window (BVW).

All of the above calculations are done by the Atomistix Toolkit (ATK) package,[33–36] which is based on the DFT + NEGF method. The exchange and correlation energies are dealt with the spin generalized gradient approximation (SGGA) according to the Perdew, Burke, and Ernzerhof (PBE) parameterization.[37] The valence electron wavefunctions of all atoms are expanded by a double-ζ plus polarization (DZP) basis set. The electron–ion interaction is modeled by the Troullier–Martins norm-conserving pseudopotentials.[38] A density mesh cutoff energy of 100 Hartree (1 Hartree $= 4.3597\times10^{-18}$ J) is adopted, while the k-point grids used for structural optimization and spin-polarized transport calculations are $5\times5\times21$ and $5\times5\times100$, respectively.

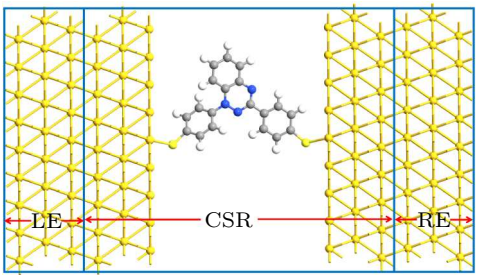


Fig. 1. The model structure of the designed molecular spintronic device (MSD), in which a Blatter radical is coupled covalently to two gold electrodes via sulfur atom. The gray, blue, white, yellow, and golden spheres represent carbon, nitrogen, hydrogen, sulfur, and gold atoms, respectively. The model is divided into three regions: the left electrode (LE), the central scattering region (CSR), and the right electrode (RE).

3. Results and discussion

Figure 2 plots the calculated spin-resolved current–voltage (I–V) curves in the bias voltage range from -1.2 V to 1.2 V. As one can see, the spin-up current $I_{\rm up}$ always increases rapidly at forward bias voltage, while it increases rapidly (before -0.4 V) and then stabilizes to about 840 nA at backward bias voltage. Due to the obvious $I_{\rm up}$ flowing through the device at both forward and backward bias voltages, it is difficult for the $I_{\rm up}$ to present good spin-rectifying effect. In contrast to the case of $I_{\rm up}$, the spin-down current $I_{\rm dn}$ is strongly suppressed in the whole backward bias voltage range and the forward bias voltage range before 0.2 V, making it difficult to pass through the device. When the forward bias voltage is higher than 0.2 V, the $I_{\rm dn}$ begins to increase rapidly. At 0.3 V, its magnitude is almost equal to that of the $I_{\rm up}$. With the further increase of forward bias voltage, the $I_{\rm dn}$ is larger than the $I_{\rm up}$. When the forward bias voltage exceeds 0.9 V, the magnitude of $I_{\rm dn}$ is exactly equal to that of the $I_{\rm up}$. Obviously, the $I_{\rm dn}$ exhibits good spin-rectifying effect since its magnitude at forward bias voltage is much larger than that at backward bias voltage. Meantime, because the $I_{\rm up}$ is much higher than $I_{\rm dn}$ at backward bias voltage, the designed device exhibits excellent spin-filtering effect at backward bias voltage.

To quantify the observed spin-rectifying effect, we define the spin-rectifying ratio (SRR) as follows: ${\rm SRR} = I_{\sigma,+}/I_{\sigma,-}$. Here, $I_{\sigma,+}$ and $I_{\sigma,-}$ are the spin-resolved ($\sigma = {\rm up/dn}$ represents the spin-up/spin-down) forward and backward currents, respectively. Figure 3(a) plots the SRR as a function of the applied bias voltage. Obviously, the rectifying performance of $I_{\rm up}$ is very low, with a maximum SRR of no more than 3.5. On the contrary, the $I_{\rm dn}$ exhibits excellent rectifying performance. In particular, between 0.4 V and 0.8 V, the

SRR of I_{dn} is greater than 109, with a maximum of 116 occurring at 0.6 V. To quantify the observed spin-filtering effect, we define the spin-filtering efficiency (SFE) as follows: $\text{SFE} = [(I_{up} - I_{dn})/(I_{up} + I_{dn})] \times 100\%$. Especially, we calculate the zero-bias voltage SFE using the corresponding spin-resolved zero-bias voltage transmission coefficient at the E_F since all currents disappear at zero bias voltage. Figure 3(b) plots the SFE as a function of the applied bias voltage. It can be seen that the designed MSD has high performance of spin-filtering in the whole backward bias voltage range. In particular, between -0.8 V and 0 V, the SFE is greater than 95% , with a maximum of 97.7% occurring at -0.2 V. With the increase of backward bias voltage, the SFE decreases slowly, but still reaches about 87.7% at -1.2 V. In contrast, with the increase of forward bias voltage, the SFE first decreases sharply. At 0.3 V it has fallen to about 4.4%. As the forward bias voltage increases further, the SFE increases to about -30% at 0.4 V, and then decreases again. When the forward bias voltage exceeds 0.9 V, the SFE drops to zero and the spin-filtering behavior vanishes.

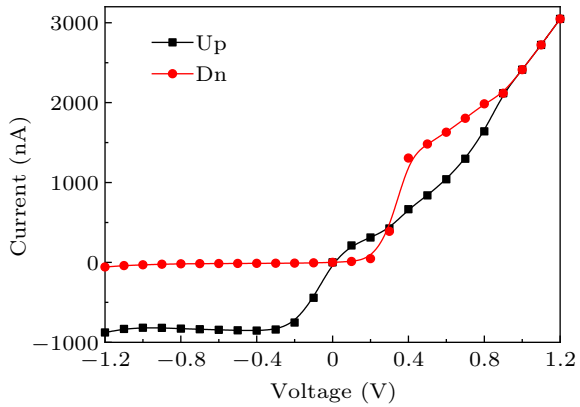


Fig. 2. Calculated spin-resolved current–voltage (I–V) curves. The black curve with squares is for the spin-up (Up) electrons and the red curve with circles is for the spin-down (Dn) electrons.

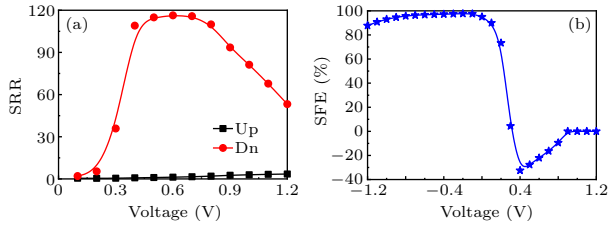


Fig. 3. (a) Calculated spin-rectifying ratio (SRR) as a function of the applied bias voltage. The black curve with squares is for the spin-up electrons and the red curve with circles is for the spin-down electrons. (b) Calculated spin-filtering efficiency (SFE)) as a function of the applied bias voltage.

According to the Eq. (1), the spin-resolved current through the device is determined by the integral of $T_\sigma(E,V)$ in the BVW. To elucidate the observed spin-rectifying and spin-filtering effects, figures 4(a) and 4(b) plot the spin-up and spin-down bias voltage-dependent transmission spectra, respectively. Here, the two dashed white lines indicate the μ_L and μ_R, respectively, and the energy range between them is the BVW. It can be seen that there is a weak spin-up transmission peak at -0.07 eV just below the E_F (Fig. 4(a)), and a weak spin-down transmission peak at 0.37 eV above the E_F (Fig. 4(b)) in equilibrium state. Meantime, one can see that in non-equilibrium state, the two transmission peaks move with the shift of μ_L, regardless of whether the forward or backward bias voltage is applied. For the spin-up case, as shown in Fig. 3(a), when the forward bias voltage is applied, the tail of spin-up transmission peak just below the E_F in equilibrium state rapidly enters the forward BVW (FBVW), and then this spin-up transmission peak completely enters the FBVW with the increase of forward bias voltage. During this process, the strength of this spin-up transmission peak increases continuously, leading the I_{up} to increase continuously at forward bias voltage. When the backward bias voltage is applied, the spin-up transmission peak just below the E_F in equilibrium state quickly enters the backward BVW (BBVW), and its strength decreases slightly at first and then remains basically unchanged after -0.4 V. This causes the I_{up} to increase rapidly at first and then stabilize to about 840 nA at backward bias voltage. Because there is obvious I_{up} at both forward and backward bias voltages, the spin-rectifying performance of I_{up} is very weak. For the spin-down case, as shown in Fig. 4(b), when the forward bias voltage is applied, the spin-down transmission peak at 0.37 eV above the E_F in equilibrium state cannot enter the FBVW at first since it is far away from the E_F. Therefore, the I_{dn} at this stage is very weak, much less than the I_{up}. Therefore, the device at this stage exhibits very high positive SFEs. With the increase of forward bias voltage, this spin-down transmission peak moves toward the FBVW following the μ_L, and begins to enter the FBVW at 0.3 V. At this point, the magnitude of I_{dn} has almost caught up with the magnitude of the I_{up}, resulting in a rapid reduction of SFE to 4.4%. After 0.3 V, this spin-down transmission peak completely enters the FBVW. Between 0.3 V and 0.9 V, the magnitude of the I_{dn} exceeds the magnitude of the I_{up}, resulting in negative SFEs in this forward bias voltage range. Meantime, with the increase of forward bias voltage, the strength of this spin-down transmission peak increases continuously. Comparing Figs. 4(b) and 4(a), one can see that when the forward bias voltage exceeds 0.9 V, the spin-down transmission peak becomes exactly the same as the spin-up transmission peak, resulting in a reduction of SFE to zero, and the device no longer has any spin filtering performance. When the backward bias voltage is applied, the spin-down transmission peak at 0.37 eV above the E_F in equilibrium state never enters the FBVW, resulting in a strong suppression of the I_{dn} in the whole backward bias voltage range. As a result, the I_{dn} shows excellent spin-rectifying performance and the designed device exhibits high-performance spin-filtering effect at backward bias volt-

age.

In general, the position of the transmission peak is determined by the position of the energy level of the molecular projected self-consistent Hamiltonian (MPSH)[39] orbital, and the strength of the transmission peak is determined by the delocalization extent of the MPSH orbital. Figure 5 plots the spin-polarized MPSH levels as a function of the applied bias voltage. Here, the two dashed blue lines indicate the μ_L and μ_R, respectively, and the energy range between them is the BVW. Obviously, there is a spin-up MPSH MO at −0.08 eV and a spin-down MPSH MO at 0.35 eV in equilibrium state. As shown by their spatial distribution in Fig. 6, the electronic states of these two MPSH MOs cannot spread to the anchoring sulfur atom on the right at 0 V (For clarity, the electron state on the right anchoring sulfur atom is amplified and displayed in the cirlcle.). Therefore, these two MPSH MOs can only cause two weak spin-polarized transmission peaks at the corresponding energy positions around the E_F. At the same time, in contrast to the absence of electron state on the right anchoring sulfur atom, the left anchoring sulfur atom has significant electron state, indicating that the left sulfur atom has a stronger coupling with the LE than the right sulfur atom with the RE. Thus, when a bias voltage is applied, as shown in Fig. 5, these two MPSH MOs move with the shift of μ_L. And as shown in Figs. 3(a) and 3(b), the spin-polarized transmission peaks originating from these two MPSH MOs also move with the shift of μ_L. Also, as shown by the spatial distribution of two MPSH MOs in Fig. 6, when the forward bias voltage (1.2 V) is applied, a small number of electron states appear on the right sulfur atom, implying an increased delocalization of the two MPSH MOs. This results in the strength of the corresponding transmission peaks increases gradually with the increase of applied forward bias voltage. In contrast, when the backward bias voltage (−1.2 V) is applied, the electronic states of two MPSH MOs still cannot spread to the right sulfur atom, that is, the delocalization of the two MPSH MOs at backward bias voltage is not enhanced. Therefore, compared with the equilibrium state, the strength of transmission peaks originating from these two MPSH MOs at backward bias voltage has little change.

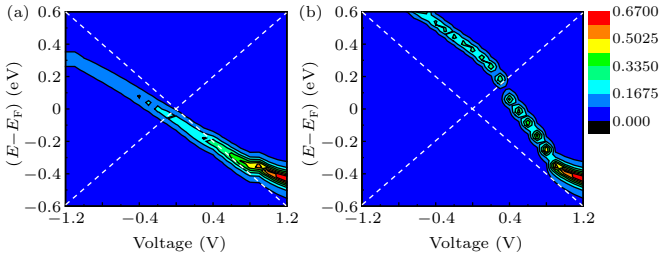


Fig. 4. (a) Calculated the spin-up bias voltage-dependent transmission spectra. (b) Calculated the spin-down bias voltage-dependent transmission spectra. Here, the two dashed white lines indicate the μ_L and μ_R, respectively, and the energy range between them is the bias voltage window (BVW).

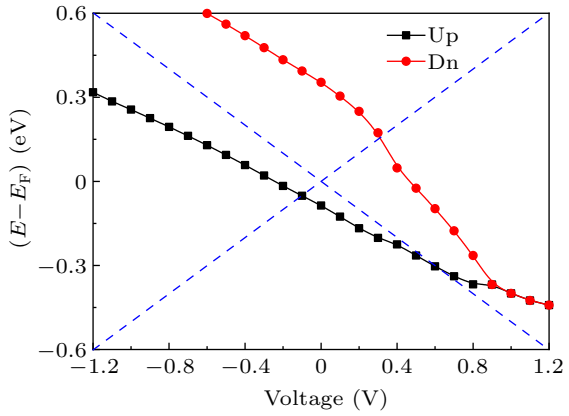


Fig. 5. Calculated spin-polarized molecular projected self-consistent Hamiltonian (MPSH) orbital levels as a function of the applied bias voltage. Here, the two dashed blue lines indicate the μ_L and μ_R, respectively, and the energy range between them is the BVW.

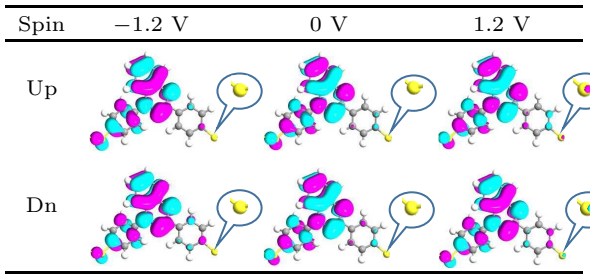


Fig. 6. Calculated spatial distribution of two spin-resolved MPSH orbitals around the Fermi level at −1.2 V, 0 V, and 1.2 V. For clarity, the electron state on the right anchoring sulfur atom is amplified and displayed in the cirlcle. The isosurface level is 0.05 $|e|/\text{Å}^3$.

4. Conclusion

In conclusion, we have designed a Blatter radical-based MSD and investigated its spin-polarized transport properties using the density functional theory combined with the non-equilibrium Green's function technique. The spin-polarized transport calculations demonstrate that the spin-down current has high-performance spin-rectifying behavior, and the designed device exhibits excellent spin-filtering effect at backward bias voltage. The results are explained by the spin-resolved bias voltage-dependent transmission spectra, the energy levels of corresponding molecular projected self-consistent Hamiltonian orbitals, and their spatial distributions. The results show that the Blatter radical has great application prospects in molecular spintronics.

Acknowledgment

Project supported by the Natural Science Foundation of Shandong Province, China (Grant No. ZR2021MA059).

References

[1] Majumder C, Mizuseki H and Kawazoe Y 2001 *J. Phys. Chem. A* **105** 9454
[2] Bu D, Xiong Y, Tan Y N, Meng M and Liu C Y 2018 *Chem. Commun.* **54** 3632
[3] Kondo H, Nara J and Ohno T 2011 *J. Phys. Chem. C* **115** 6886

[4] Pour M M, Lashkov A, Radocea A, Liu X, Sun T, Lipatov A, Korlacki R A, Shekhirev M, Aluru N R, Lyding J W, Sysoev V and Sinitskii A 2017 *Nat. Commun.* **8** 820

[5] Yin X, Zang Y, Zhu L, Low J Z, Liu Z F, Cui J, Neaton J B, Venkataraman L and Cammpos L M 2017 *Sci. Adv.* **3** eaao2615

[6] Chandler H J, Stefanou M, Campbell E E B and Schaub R 2019 *Nat. Commun.* **10** 2283

[7] Chen J, Reed M A, Rawlett A M and Tour J M 1999 *Science* **286** 1550

[8] Zhao P, Liu D S, Zhang Y, Su Y, Liu H Y, Li S J and Chen G 2012 *J. Phys. Chem. C* **116** 7968

[9] Aviram A and Ratner M A 1974 *Chem. Phys. Lett.* **29** 277

[10] Wolf S A, Awschalom D D, Buhrman R A, Daughton J A, von Molnár S, Roukes M L, Chtchelkanova A Y and Treger D M 2001 *Science* **294** 1488

[11] Rocha A R, García-suárez V M, Bailey S W, Lambert C J, Ferrer J and Sanvito S 2005 *Nat. Mater.* **4** 335

[12] Ferrer J and García-suárez V M 2009 *J. Mater. Chem.* **19** 1696

[13] Lakshmi S, Roche S and Cuniberti G 2009 *Phys. Rev. B* **80** 193404

[14] Herrmann C, Rolomon G C and Ratner M A 2010 *J. Am. Chem. Soc.* **132** 3682

[15] Smeu M and DiLabio G A 2010 *J. Phys. Chem. C* **114** 17874

[16] Shil S, Bhattacharya D, Misra A and Klein D J 2015 *Phys. Chem. Chem. Phys.* **17** 23378

[17] Bajaj A, Kaur P, Sud A, Berritta M and Ali M E 2020 *J. Phys. Chem. C* **124** 24361

[18] Smeu M, Monti O L A and McGrath D 2021 *Phys. Chem. Chem. Phys.* **23** 24106

[19] Li Y F, Zhao P, Xu Z and Chen G 2022 *Chem. Phys. Lett.* **794** 139515

[20] Blatter H M and Lukaszewski H 1968 *Tetrahedron Lett.* **9** 2701

[21] Grant J A, Lu Z, Tucker D E, Hockin B M, Yufit D S, Fox M A, Kataky R, Chechik V and O'Donoghue A C 2017 *Nat. Commun.* **8** 15088

[22] Ji Y, Long L and Zheng Y 2020 *Mater. Chem. Front.* **4** 3433

[23] Rogers F J M, Norcott P L and Coote M L 2020 *Org. Biomol. Chem.* **18** 8255

[24] Yan B, Cramen J, McDonald R and Frank N L 2011 *Chem. Commun.* **47** 3201

[25] Ciccullo F, Gallagher N M, Geladari O, Chassé T, Rajca A and Casu M B 2016 *ACS Appl. Mater. Interfaces* **8** 1805

[26] Demetriou M, Berezin A A, Koutentis P A and Krasia-Christoforou T 2014 *Polym. Int.* **63** 674

[27] Kuznetsova Y L, Vavilova A S, Malysheva Y B, Lopatin M A, Grishin I D, Burdyukova T O, Zaburdaeva E A, Polozov E Y and Fedorov A Y 2020 *Russ. Chem. Bull.* **69** 1470

[28] Ciccullo F, Calzolari A, Bader K, Neugebauer P, Gallagher N M, Rajca A, van Slageren J and Casu M B 2019 *ACS Appl. Mater. Interfaces* **11** 1571

[29] Sellers H, Ulman A, Shnidman Y and Eilers J E 1993 *J. Am. Chem. Soc.* **115** 9389

[30] Larsen N B, Biebuyck H, Delamarche E and Michel B 1997 *J. Am. Chem. Soc.* **119** 3017

[31] Damle P, Rakshit T, Paulsson M and Datta S 2002 *IEEE Trans. Nanotechnol.* **1** 145

[32] Büttiker M, Imry Y, Landauer R and Pinhas S 1985 *Phys. Rev. B* **31** 6207

[33] Taylor J, Guo H and Wang J 2001 *Phys. Rev. B* **63** 121104

[34] Taylor J, Guo H and Wang J 2001 *Phys. Rev. B* **63** 245407

[35] Brandbyge M, Mozos J L, Ordejón P, Taylor J and Stokbro K 2002 *Phys. Rev. B* **65** 165401

[36] Soler J M, Artacho E, Gale J D, García A, Junquera J, Ordejón P and Sánchez-Portal D 2002 *J. Phys.: Condens. Matter* **14** 2745

[37] Perdew J P, Burke K and Ernzerhof M 1996 *Phys. Rev. Lett.* **77** 3865

[38] Troullier N and Martins J 1991 *Phys. Rev. B* **43** 1993

[39] Stokbro K, Taylor J, Brandbyge M, Mozos J L and Ordejón P 2003 *Comput. Mater. Sci.* **27** 151